CHAPTER

Interfacial Cracks between Two Dissimilar Solids

8

Engineering structures may be made of two or more dissimilar materials. Examples include structural composites, coating-substrate systems, and multilayered electronic devices. In a medium consisting of two or more materials with distinct properties, failure often initiates at the interfaces. Thus, the behavior of interface cracks is of interest. A distinct feature of a crack along the interface between two dissimilar elastic materials is that the stress field possesses an oscillatory character of the type $r^{-1/2+i\epsilon}$, where r is the radial distance from the crack tip and ϵ is a bimaterial constant. Mathematically, the oscillation behavior of the near-tip stress and displacement fields implies overlap of the upper and lower crack surfaces near the tip, which is physically inadmissible. Nevertheless, fracture criteria based on the oscillatory fields have been proposed and may be used to predict failure of interfaces because the region of the two crack faces in contact is extremely small compared with the crack length for most engineering applications.

8.1 CRACK TIP FIELDS

As in the case for homogeneous materials, the crack tip stress and displacement fields also play a central role in establishing fracture parameters for investigating interface fracture. The asymptotic eigenfunction expansion method can still be used to analyze the interface crack tip fields but the characteristic equations for determining the eigenvalue or the stress singularity index is much more complex due to the material property mismatch along the interface. In the following, Williams' solution for in-plane deformation is first presented. The solution approach is subsequently applied to the antiplane deformation case. Finally, Dundurs' parameters for describing bimaterial mismatch are introduced.

8.1.1 Asymptotic Stress and Displacement Fields

In analyzing the asymptotic crack tip stress and displacement fields, it is sufficient to consider a semi-infinite crack lying at the interface between two dissimilar homogeneous materials as shown in Figure 8.1. The upper material (material 1) has a shear modulus μ_1 and a Poisson's ratio ν_1 and the lower material (material 2) possesses

Fracture Mechanics. DOI: 10.1016/B978-0-12-385001-0.00008-0
© 2012 Elsevier Inc. All rights reserved.

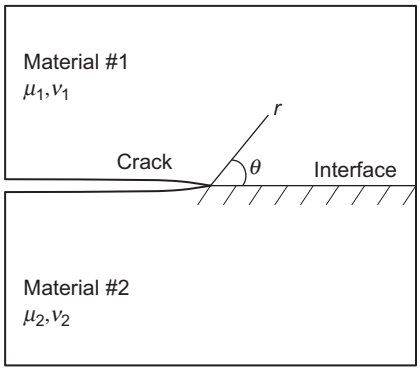

FIGURE 8.1

A crack at the interface between two dissimilar homogeneous materials.

the properties μ_2 and ν_2. This problem was first analyzed by Williams [8-1] using an eigenfunction expansion method.

Let the stress functions in material 1 and material 2 be denoted by ϕ_1 and ϕ_2, respectively. These functions satisfy the following biharmonic equations:

$$\nabla^2 \nabla^2 \phi_j = 0, \quad j = 1, 2 \tag{8.1}$$

where

$$\nabla^2 = \frac{\partial^2}{\partial r^2} + \frac{1}{r}\frac{\partial}{\partial r} + \frac{1}{r^2}\frac{\partial^2}{\partial \theta^2}$$

is the Laplacian operator with (r, θ) being the polar coordinates centered at the crack tip and $\theta = 0$ along the interface, as shown in Figure 8.1. The boundary conditions of the problem consist of the crack surface ($\theta = \pm\pi$) traction-free conditions,

$$\begin{aligned} (\sigma_{\theta\theta})_1 = (\sigma_{r\theta})_1 = 0, \quad \theta = \pi \\ (\sigma_{\theta\theta})_2 = (\sigma_{r\theta})_2 = 0, \quad \theta = -\pi \end{aligned} \tag{8.2}$$

and the stress and displacement continuity conditions along the interface ($\theta = 0$),

$$\begin{aligned} (\sigma_{\theta\theta})_1 &= (\sigma_{\theta\theta})_2, \quad \theta = 0 \\ (\sigma_{r\theta})_1 &= (\sigma_{r\theta})_2, \quad \theta = 0 \\ (u_r)_1 &= (u_r)_2, \quad \theta = 0 \\ (u_\theta)_1 &= (u_\theta)_2, \quad \theta = 0 \end{aligned} \tag{8.3}$$

A general solution to Eq. (8.1) can be obtained using the method of separation of variables by assuming

$$\phi_j = r^{\lambda+1} F_j(\theta), \quad j = 1,2 \tag{8.4}$$

where λ is the eigenvalue to be determined and $F_j(\theta)$ are the eigenfunctions. It is noted that the same value of λ is assumed for both material 1 and material 2, which is a result of continuity requirements Eq. (8.3). Substitution of Eq. (8.4) into Eq. (8.1) yields

$$\frac{d^4 F_j(\theta)}{d\theta^4} + 2(\lambda^2+1)\frac{d^2 F_j(\theta)}{d\theta^2} + (\lambda^2-1)^2 F_j(\theta) = 0, \quad j = 1,2$$

The differential equations here have the following solutions:

$$\begin{aligned} F_j(\theta) = {} & a_j \sin(\lambda+1)\theta + b_j \cos(\lambda+1)\theta \\ & + c_j \sin(\lambda-1)\theta + d_j \cos(\lambda-1)\theta, \quad j = 1,2 \end{aligned} \tag{8.5}$$

where a_j, b_j, c_j, and d_j $(j = 1,2)$ are unknown constants. The corresponding stresses are

$$\begin{aligned} (\sigma_{rr})_j &= \frac{1}{r^2}\frac{\partial^2 \phi_j}{\partial \theta^2} + \frac{1}{r}\frac{\partial \phi_j}{\partial r} = r^{\lambda-1}\left[F_j''(\theta) + (\lambda+1)F_j(\theta)\right] \\ (\sigma_{\theta\theta})_j &= \frac{\partial^2 \phi_j}{\partial r^2} = r^{\lambda-1}\lambda(\lambda+1)F_j(\theta) \\ (\sigma_{r\theta})_j &= -\frac{1}{r}\frac{\partial^2 \phi_j}{\partial r \partial \theta} + \frac{1}{r^2}\frac{\partial \phi_j}{\partial \theta} = -\lambda r^{\lambda-1} F_j'(\theta) \end{aligned} \tag{8.6}$$

and the displacement components are given by

$$\begin{aligned} (u_r)_j = {} & \frac{1}{2\mu_j} r^{\lambda}\{-(\lambda+1)F_j(\theta) + (1+\kappa_j)[c_j \sin(\lambda-1)\theta \\ & + d_j \cos(\lambda-1)\theta]\} \\ (u_\theta)_j = {} & \frac{1}{2\mu_j} r^{\lambda}\{-F_j'(\theta) - (1+\kappa_j)[c_j \cos(\lambda-1)\theta \\ & - d_j \sin(\lambda-1)\theta]\} \end{aligned} \tag{8.7}$$

where

$$\kappa_j = \begin{cases} 3 - 4\nu_j & \text{for plane strain} \\ \dfrac{3-\nu_j}{1+\nu_j} & \text{for plane stress} \end{cases}$$

Substitution of these stress and displacement expressions into the boundary conditions Eqs. (8.2) and (8.3) leads to the following eight simultaneous equations for the constants a_j, b_j, c_j, and d_j $(j = 1,2)$:

$$a_1 \sin(\lambda+1)\pi + b_1 \cos(\lambda+1)\pi + c_1 \sin(\lambda-1)\pi + d_1 \cos(\lambda-1)\pi = 0$$
$$-a_2 \sin(\lambda+1)\pi + b_2 \cos(\lambda+1)\pi - c_2 \sin(\lambda-1)\pi + d_2 \cos(\lambda-1)\pi = 0$$

$$a_1(\lambda+1)\cos(\lambda+1)\pi - b_1(\lambda+1)\sin(\lambda+1)\pi + c_1(\lambda-1)\cos(\lambda-1)\pi - d_1(\lambda-1)\sin(\lambda-1)\pi = 0$$

$$a_2(\lambda+1)\cos(\lambda+1)\pi + b_2(\lambda+1)\sin(\lambda+1)\pi + c_2(\lambda-1)\cos(\lambda-1)\pi + d_2(\lambda-1)\sin(\lambda-1)\pi = 0$$

$$b_1 + d_1 = b_2 + d_2$$
$$a_1(\lambda+1) + c_1(\lambda-1) = a_2(\lambda+1) + c_2(\lambda-1)$$
$$(1+\kappa_1)c_1 = \frac{\mu_1}{\mu_2}(1+\kappa_2)c_2 + \left(\frac{\mu_1}{\mu_2} - 1\right)[(\lambda+1)a_2 + (\lambda-1)c_2]$$
$$(1+\kappa_1)d_1 = \frac{\mu_1}{\mu_2}(1+\kappa_2)d_2 - \left(\frac{\mu_1}{\mu_2} - 1\right)(\lambda+1)[b_2 + d_2]$$

The existence of a nontrivial solution for the four unknowns a_j, b_j, c_j, and d_j requires that the determinant of the system of equations vanish. This yields the following characteristic equation to determine the eigenvalue λ:

$$\cot^2 \lambda\pi + \left[\frac{\frac{\mu_1}{\mu_2}(1+\kappa_2) - (1+\kappa_1) - 2\left(\frac{\mu_1}{\mu_2} - 1\right)}{\frac{\mu_1}{\mu_2}(1+\kappa_2) + (1+\kappa_1)}\right]^2 = 0 \tag{8.8}$$

Except for the case of a homogeneous solid ($\mu_1 = \mu_2$ and $\nu_1 = \nu_2$), the preceding equation has only complex solutions for λ. Let

$$\lambda = \lambda_R + i\lambda_I$$

Substitution of the λ into Eq. (8.8) yields two equations for λ_R and λ_I:

$$\frac{(\tan^2 \lambda_R\pi + 1)\tanh \lambda_I\pi}{\tan^2 \lambda_R\pi + \tanh^2 \lambda_I\pi} = \pm \frac{\frac{\mu_1}{\mu_2}(1+\kappa_2) - (1+\kappa_1) - 2\left(\frac{\mu_1}{\mu_2} - 1\right)}{\frac{\mu_1}{\mu_2}(1+\kappa_2) + (1+\kappa_1)}$$

$$\frac{\tan\lambda_R\pi\left(1-\tanh^2\lambda_I\pi\right)}{\tan^2\lambda_R\pi+\tanh^2\lambda_I\pi}=0 \tag{8.9}$$

Mathematically, these equations permit two sets of solutions:

1. It is clear that the second equation in Eq. (8.9) can be satisfied if $\tan\lambda_R\pi=0$. Now we obtain

$$\lambda_R=n,\quad n=0,1,2,\ldots$$

$$\lambda_I=\pm\frac{1}{\pi}\coth^{-1}\left[\frac{\frac{\mu_1}{\mu_2}(1+\kappa_2)-(1+\kappa_1)-2\left(\frac{\mu_1}{\mu_2}-1\right)}{\frac{\mu_1}{\mu_2}(1+\kappa_2)+(1+\kappa_1)}\right]$$

It is seen from the λ_R and the stress expressions in Eq. (8.6) that only one value of λ_R corresponding to $n=0$ will produce stress singularity at the crack tip. With this value, the stresses in Eq. (8.6) near the crack tip vary with r as

$$\sigma_{rr},\sigma_{\theta\theta},\sigma_{r\theta}\sim\frac{1}{r}\begin{pmatrix}\sin\\ \cos\end{pmatrix}(\lambda_I\ln r)$$

It can be shown that these stresses lead to infinite strain energy in any small region containing the crack tip ($r\to 0$), which is physically unrealistic.

2. The second equation in Eq. (8.9) can also be satisfied if $\tan\lambda_R\pi=\infty$. We then obtain the second set of the eigenvalue:

$$\lambda_R=\frac{2n-1}{2},\quad n=1,2,3,\ldots$$

$$\lambda_I=\pm\frac{1}{\pi}\tanh^{-1}\left[\frac{\frac{\mu_1}{\mu_2}(1+\kappa_2)-(1+\kappa_1)-2\left(\frac{\mu_1}{\mu_2}-1\right)}{\frac{\mu_1}{\mu_2}(1+\kappa_2)+(1+\kappa_1)}\right]$$

Using the relation

$$\tanh^{-1}\frac{x}{b}=\frac{1}{2}\ln\frac{b+x}{b-x}$$

we can express the eigenvalues in the form

$$\lambda=\left(n-\frac{1}{2}\right)\pm i\epsilon,\quad n=1,2,\ldots \tag{8.10}$$

where

$$\epsilon=\frac{1}{2\pi}\ln\left[\left(\frac{\kappa_1}{\mu_1}+\frac{1}{\mu_2}\right)\Big/\left(\frac{\kappa_2}{\mu_2}+\frac{1}{\mu_1}\right)\right] \tag{8.11}$$

It can be seen from Eqs. (8.6) and (8.10) that only the eigenvalue for $n = 1$ produces singular stresses at the crack tip. The $\pm$ sign in Eq. (8.10) is not essential because ϵ changes sign if material 1 and 2 are switched. The eigenvalue is thus chosen as $\lambda = 1/2 + i\epsilon$ for the crack tip singular stresses, which vary with r as

$$\sigma_{rr}, \sigma_{\theta\theta}, \sigma_{r\theta} \sim r^{-1/2+i\epsilon}$$

and the crack tip displacements have the asymptotic form as $r \to 0$:

$$u_r, u_\theta \sim r^{1/2+i\epsilon}$$

Because

$$r^{i\epsilon} = e^{i\epsilon \ln r} = \cos(\epsilon \ln r) + i \sin(\epsilon \ln r)$$

the crack tip stresses and displacements can also be expressed as

$$\sigma_{rr}, \sigma_{\theta\theta}, \sigma_{r\theta} \sim r^{-1/2} [\cos(\epsilon \ln r) + i \sin(\epsilon \ln r)] \tag{8.12}$$

$$u_r, u_\theta \sim r^{1/2} [\cos(\epsilon \ln r) + i \sin(\epsilon \ln r)] \tag{8.13}$$

A few comments on the stress and displacement fields Eqs. (8.12) and (8.13) are in order:

1. The stress singularity of the type $r^{-1/2+i\epsilon}$ and the displacements' dependence on r according to $r^{1/2+i\epsilon}$ near the crack tip implies that the stresses and the displacements exhibit an oscillating character as they change sign indefinitely when r approaches zero.
2. The oscillatory nature of the displacement field implies interpenetration of two crack faces, which is physically inadmissible. In other words, the crack faces must come in contact near the tip. This will be discussed in Sections 8.3 and 8.7.
3. In the special case of $\epsilon = 0$, the oscillatory terms disappear, and the near-tip stress and displacement fields have exactly the same forms as those for homogeneous materials. ϵ is sometimes called the oscillation index.

8.1.2 Mode III Case

An interface crack in a Mode III field is a special case wherein no stress oscillation occurs as opposed to the general in-plane modes cases. Consider the bimaterial crack problem of Figure 8.1 with the medium subjected to anti-plane shear loading. The only nonvanishing displacements are $w_j = w_j(r, \theta)$, which satisfy the harmonic equations

$$\nabla^2 w_j = \frac{\partial^2 w_j}{\partial r^2} + \frac{1}{r}\frac{\partial w_j}{\partial r} + \frac{1}{r^2}\frac{\partial^2 w_j}{\partial \theta^2} = 0, \quad j = 1, 2 \tag{8.14}$$

The nonvanishing stress components are given by

$$(\sigma_{rz})_j = \mu_j \frac{\partial w_j}{\partial r}, \quad (\sigma_{\theta z})_j = \mu_j \frac{1}{r} \frac{\partial w_j}{\partial \theta} \tag{8.15}$$

The boundary conditions for the Mode III crack problem consist of the traction-free conditions on the crack surfaces,

$$\begin{aligned} (\sigma_{\theta z})_1 &= 0, \quad \theta = \pi \\ (\sigma_{\theta z})_2 &= 0, \quad \theta = -\pi \end{aligned} \tag{8.16}$$

and the continuity of stresses and displacements along the interface,

$$\begin{aligned} (\sigma_{\theta z})_1 &= (\sigma_{\theta z})_2, \qquad \theta = 0 \\ w_1 &= w_2, \qquad \theta = 0 \end{aligned} \tag{8.17}$$

Following the treatment for the in-plane crack problem described before, the displacements and stresses near the crack tip may be expressed in the following forms after the governing Eq. (8.14) is satisfied:

$$w_j(r,\theta) = r^{\lambda}[A_j \sin(\lambda\theta) + B_j \cos(\lambda\theta)]$$

$$\begin{aligned} (\sigma_{rz})_j &= \mu_j \lambda r^{\lambda-1}[A_j \sin(\lambda\theta) + B_j \cos(\lambda\theta)] \\ (\sigma_{\theta z})_j &= \mu_j \lambda r^{\lambda-1}[A_j \cos(\lambda\theta) - B_j \sin(\lambda\theta)] \end{aligned}$$

Use of the boundary conditions Eqs. (8.16) and (8.17) leads to the following equations to determine the unknown constants A_j and B_j $(j = 1,2)$:

$$\begin{aligned} \mu_1 A_1 &= \mu_2 A_2 \\ B_1 &= B_2 \end{aligned}$$

$$\begin{aligned} A_1 \cos(\lambda\pi) - B_1 \sin(\lambda\pi) &= 0 \\ \mu_1 A_1 \cos(\lambda\pi) + \mu_2 B_1 \sin(\lambda\pi) &= 0 \end{aligned}$$

A nontrivial solution of A_j and B_j exists if

$$\begin{vmatrix} \cos(\lambda\pi) & -\sin(\lambda\pi) \\ \mu_1 \cos(\lambda\pi) & \mu_2 \sin(\lambda\pi) \end{vmatrix} = 0$$

or

$$\sin(2\lambda\pi) = 0$$

Thus, the eigenvalue λ can be obtained as

$$\lambda = \lambda^{(n)} = \frac{n}{2}, \quad n = 0, \pm 1, \pm 2$$

Since $n = -1, -2, \ldots$ lead to unbounded displacement at the crack tip, they are excluded in the solution. In addition, $\lambda = 0$ is neglected since it corresponds to a rigid body motion.

Consider the class of solutions for which the displacement w is antisymmetric with respect to the crack plane (x-axis). Thus,

$$B_1 = B_2 = 0$$

and

$$\lambda^{(n)} = \frac{1}{2} + n, \quad n = 0, 1, 2, 3, \ldots \tag{8.18}$$

The displacement solution is given by

$$\begin{aligned} w_1(r,\theta) &= \sum_{n=0}^{\infty} r^{\frac{1}{2}+n} A^{(n)} \sin\left[\left(\frac{1}{2}+n\right)\theta\right] \\ w_2(r,\theta) &= \frac{\mu_1}{\mu_2} w_1(r,\theta) \end{aligned} \tag{8.19}$$

and the corresponding stresses are

$$\begin{aligned} (\sigma_{rz})_1 = (\sigma_{rz})_2 &= \mu_1 \sum_{n=0}^{\infty} \left(n+\frac{1}{2}\right) r^{n-\frac{1}{2}} A^{(n)} \sin\left[\left(n+\frac{1}{2}\right)\theta\right] \\ (\sigma_{\theta z})_1 = (\sigma_{\theta z})_2 &= \mu_1 \sum_{n=0}^{\infty} \left(n+\frac{1}{2}\right) r^{n-\frac{1}{2}} A^{(n)} \cos\left[\left(n+\frac{1}{2}\right)\theta\right] \end{aligned} \tag{8.20}$$

It can be seen from these stress expressions that $n = 0$ yields the inverse square root $(1/\sqrt{r})$ singularity and the crack tip singular stress field can be expressed as

$$\begin{aligned} (\sigma_{rz})_1 = (\sigma_{rz})_2 &= \frac{1}{2}\mu_1 A^{(0)} r^{-1/2} \sin\frac{\theta}{2} \\ (\sigma_{\theta z})_1 = (\sigma_{\theta z})_2 &= \frac{1}{2}\mu_1 A^{(0)} r^{-1/2} \cos\frac{\theta}{2} \end{aligned} \tag{8.21}$$

It is clear that no oscillatory behavior is seen in the Mode III stress field.

8.1.3 Dundurs' Parameters

Dundurs [8-2] introduced two bimaterial parameters called α and β to describe the material property mismatch:

$$\begin{aligned}\alpha &= \frac{\mu_1(\kappa_2+1)-\mu_2(\kappa_1+1)}{\mu_1(\kappa_2+1)+\mu_2(\kappa_1+1)}\\ \beta &= \frac{\mu_1(\kappa_2-1)-\mu_2(\kappa_1-1)}{\mu_1(\kappa_2+1)+\mu_2(\kappa_1+1)}\end{aligned} \tag{8.22}$$

Clearly, $\alpha=\beta=0$ if no material property mismatch occurs. For general bimaterial systems with positive Poisson's ratios, $|\alpha|\le 1$. The equality takes place when $\mu_2/\mu_1\to\infty$ or $\mu_2/\mu_1\to 0$. Similarly, $|\beta|\le 0.5$ and the equality occurs when $\mu_2/\mu_1\to\infty$ and $\nu_1=0$ or $\mu_2/\mu_1\to 0$ and $\nu_2=0$.

With the Dundurs parameter β, the oscillation index ϵ in the crack tip field can be expressed as

$$\epsilon=\frac{1}{2\pi}\ln\frac{1-\beta}{1+\beta} \tag{8.23}$$

8.2 COMPLEX FUNCTION METHOD AND STRESS INTENSITY FACTORS

The complex variables method of Kosolov-Muskhelishvili for homogeneous materials may still be used to obtain stresses and stress intensity factor solutions for interface cracks, although the mathematical manipulations are more complicated. The complex potential representations of stresses and displacements, Eqs. (3.23) through (3.25) in Chapter 3, now have the forms

$$\begin{aligned}(\sigma_{xx})_1+(\sigma_{yy})_1 &= 4\,\mathrm{Re}\{\psi_1'(z)\}\\ (\sigma_{yy})_1-(\sigma_{xx})_1+2i(\sigma_{xy})_1 &= 2\{\bar{z}\psi_1''(z)+\chi_1''(z)\}\\ 2\mu_1[(u_x)_1+i(u_y)_1] &= \kappa_1\psi_1(z)-z\overline{\psi_1'(z)}-\overline{\chi_1'(z)}\end{aligned} \tag{8.24}$$

for material 1 (see Figure 8.1), and

$$\begin{aligned}(\sigma_{xx})_2+(\sigma_{yy})_2 &= 4\,\mathrm{Re}\{\psi_2'(z)\}\\ (\sigma_{yy})_2-(\sigma_{xx})_2+2i(\sigma_{xy})_2 &= 2\{\bar{z}\psi_2''(z)+\chi_2''(z)\}\\ 2\mu_2[(u_x)_2+i(u_y)_2] &= \kappa_2\psi_2(z)-z\overline{\psi_2'(z)}-\overline{\chi_2'(z)}\end{aligned} \tag{8.25}$$

for material 2 (see Figure 8.1).

It follows from the preceding expressions and the crack tip stress field Eq. (8.12) that near the crack tip,

$$\psi_1'(z) \sim (z-L)^{-1/2-i\epsilon}, \quad z \to L$$

where $z = L$ represents the crack tip. Rice and Sih [8-3] thus defined a complex stress intensity factor by

$$k_1 - ik_2 = 2\sqrt{2}e^{\pi\epsilon} \lim_{z\to L}(z-L)^{1/2+i\epsilon}\psi_1'(z) \tag{8.26}$$

8.2.1 Stress Intensity Factor Solutions for Two Typical Crack Problems

Rice and Sih [8-3] solved two typical interface crack problems as shown in Figures 8.2 and 8.3. A detailed description for the solution procedure is not provided here. For a crack of length $2a$ at the interface between two semi-infinite media subjected to remote uniform tension σ_{yy}^{∞} and shear σ_{xy}^{∞} as shown in Figure 8.2, Rice and Sih [8-3] gave the following solutions of the complex potentials:

$$\psi_1'(z) = g(z)F(z) + A$$

$$\chi_1''(z) = e^{2\pi\epsilon}\overline{g}(z)\overline{F}(z) + \left[\frac{a^2 + 2i\epsilon az}{z^2 - a^2}g(z) - zg'(z)\right]F(z) - (A + \overline{A})$$

where $F(z)$ is

$$F(z) = \frac{1}{\sqrt{z^2 - a^2}}\left(\frac{z+a}{z-a}\right)^{i\epsilon}$$

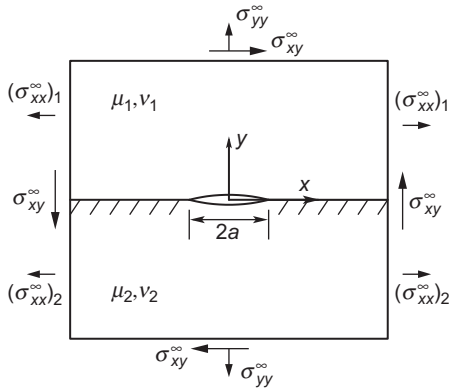

FIGURE 8.2

A crack of length $2a$ at the interface between two semi-infinite dissimilar media subjected to remote uniform loading.

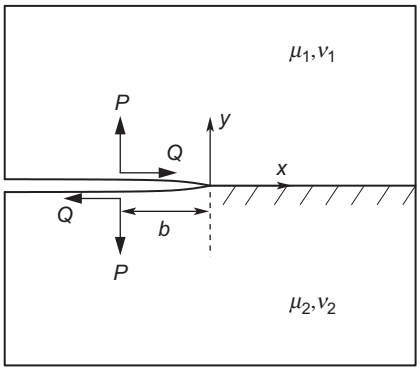

FIGURE 8.3

A semi-infinite interface crack subjected to crack surface concentrated loads.

$g(z)$ is given by

$$g(z) = \frac{\sigma_{yy}^{\infty} - i\sigma_{xy}^{\infty}}{1 + e^{2\pi\epsilon}}(z - 2i\epsilon a)$$

and A is a constant

$$A = A_1 + iA_2$$

$$A_1 = \frac{\left(\sigma_{xx}^{\infty}\right)_1 + \sigma_{yy}^{\infty}}{4} - \frac{\sigma_{yy}^{\infty}}{1 + e^{2\pi\epsilon}}$$

$$A_2 = \frac{\sigma_{xy}^{\infty}}{1 + e^{2\pi\epsilon}} + \frac{2\mu_1\omega_1^{\infty}}{1 + \kappa_1} = \frac{1}{q}\left(\frac{e^{2\pi\epsilon}\sigma_{xy}^{\infty}}{1 + e^{2\pi\epsilon}} + \frac{2\mu_2\omega_2^{\infty}}{1 + \kappa_2}\right)$$

with ω_1^{∞} and ω_2^{∞} representing the rotations at infinity in the upper and lower half planes, respectively, and q being given by

$$q = \frac{\mu_2(\kappa_1 + 1)}{\mu_1(\kappa_2 + 1)}$$

With these complex potentials, the stress intensity factors can be calculated from Eq. (8.26) (now $L = a$) as

$$\begin{aligned} k_1 &= \{\sigma\,[\cos(\epsilon \ln 2a) + 2\epsilon \sin(\epsilon \ln 2a)] + \tau\,[\sin(\epsilon \ln 2a) - 2\epsilon \cos(\epsilon \ln 2a)]\} \\ &\quad \times \sqrt{a}/\cosh(\pi\epsilon) \\ k_2 &= \{\tau\,[\cos(\epsilon \ln 2a) + 2\epsilon \sin(\epsilon \ln 2a)] - \sigma\,[\sin(\epsilon \ln 2a) - 2\epsilon \cos(\epsilon \ln 2a)]\} \\ &\quad \times \sqrt{a}/\cosh(\pi\epsilon) \end{aligned} \tag{8.27}$$

where $\sigma = \sigma_{yy}^{\infty}$ and $\tau = \sigma_{xy}^{\infty}$. Note that each stress intensity factor is induced by both tension and shear loads. The asymptotic stresses along the interface ahead of the crack tip can be expressed as

$$\left(\sigma_{yy} + i\sigma_{xy}\right)_{\theta=0} = \frac{k_1 - ik_2}{\sqrt{2r}} r^{i\epsilon} \cosh(\pi\epsilon) \tag{8.28}$$

and the near-tip relative displacements along the crack surfaces as

$$\left(u_y + iu_x\right)_{\theta=\pi} - \left(u_y + iu_x\right)_{\theta=-\pi} = \left(\frac{\kappa_1 + 1}{\mu_1} + \frac{\kappa_2 + 1}{\mu_2}\right) \frac{(k_1 - ik_2)\sqrt{2r}}{4(1 + 2i\epsilon)} r^{i\epsilon} \cosh(\pi\epsilon) \tag{8.29}$$

For a semi-infinite interface crack between two semi-infinite media subjected to concentrated forces P (tensile) and Q (shearing) at a distance b from the crack tip, as shown in Figure 8.3, Rice and Sih [8-3] gave the following solutions of the complex potentials:

$$\psi_1'(z) = z^{-1/2-i\epsilon} f(z)$$
$$\chi_1''(z) = e^{2\pi\epsilon} z^{-1/2+i\epsilon} \overline{f}(z) - z^{-1/2-i\epsilon} \left[(1/2 - i\epsilon) f(z) + z f'(z)\right]$$

where

$$f(z) = \frac{P - iQ}{2\pi e^{\pi\epsilon}} \frac{b^{1/2+i\epsilon}}{z + b}$$

With these complex potentials, the stress intensity factors are calculated as follows:

$$k_1 = \frac{1}{\pi}\sqrt{\frac{2}{b}} \left[P\cos(\epsilon \ln b) + Q\sin(\epsilon \ln b)\right]$$
$$k_2 = \frac{1}{\pi}\sqrt{\frac{2}{b}} \left[Q\cos(\epsilon \ln b) - P\sin(\epsilon \ln b)\right] \tag{8.30}$$

Note that in this example, the crack tip is at $z = L = 0$ in Eq. (8.26).

8.2.2 Further Comments on the Stress Intensity Factor Definitions

It is seen from Eq. (8.27) that the stress intensity factors depend on the measuring unit of the crack length because the $\ln(a)$ term is involved. The stress intensity factor thus is not uniquely determined. Furthermore, Mode I and Mode II deformations are coupled together even if the external loads and specimen geometry possess symmetry about the crack line. Thus, a pure Mode I or Mode II stress intensity factor can not be clearly defined. Several definitions of stress intensity factors have been proposed depending on the treatment of the coupling term $r^{i\epsilon}$ in the stress field Eq. (8.28) (e.g., in [8-3] through [8-6]). Most of these definitions differ by either a phase factor or a constant.

Hutchinson et al. [8-4] introduced a complex stress intensity factor K_h in such a way that, along the interface ahead of the crack tip, stresses are given by

$$(\sigma_{yy} + i\sigma_{xy})_{\theta=0} = \frac{K_h}{\sqrt{2\pi r}} r^{i\epsilon} \tag{8.31}$$

Comparing this expression with Eq. (8.28), we see that K_h is related to the stress intensity factor $K_r = k_1 - ik_2$ of Rice and Sih [8-3] by

$$K_r = K_h / \left[\sqrt{\pi}\cosh(\pi\epsilon)\right] \tag{8.32}$$

For the interface crack of length $2a$ in an infinite bimaterial subjected to remotely uniform stresses σ_{yy}^{∞} and σ_{xy}^{∞} as shown in Figure 8.2, the complex stress intensity factor using the definition of Hutchinson et al. [8-4] is

$$K_h = (\sigma_{yy}^{\infty} + i\sigma_{xy}^{\infty})(1 + 2i\epsilon)(2a)^{-i\epsilon}\sqrt{\pi a} \tag{8.33}$$

Similar to K_r, K_h in Eq. (8.33) is also a function of the measuring unit of the crack length. Both K_h and K_r contain a crack length–related phase term $(2a)^{-i\epsilon}$ giving rise to a complex dimension for the stress intensity factor.

Malysev and Salganik [8-5] introduced a stress intensity factor by expressing the crack tip stresses as

$$(\sigma_{yy} + i\sigma_{xy})_{\theta=0} = \frac{K_m}{\sqrt{2\pi r}} \left(\frac{r}{2a}\right)^{i\epsilon} \tag{8.34}$$

For the interface crack problem shown in Figure 8.2

$$K_m = (\sigma_{yy}^{\infty} + i\sigma_{xy}^{\infty})(1 + 2i\epsilon)\sqrt{\pi a} \tag{8.35}$$

Sun and Jih [8-6] introduced a similar stress intensity factor $K = K_1 + iK_2$ with the crack tip stress field expressed by

$$(\sigma_{yy} + i\sigma_{xy})_{\theta=0} = \frac{K}{\sqrt{2\pi r}} \left(\frac{r}{2a}\right)^{i\epsilon} \cosh(\pi\epsilon) \tag{8.36}$$

The relationship between K and K_h is

$$K_h = K(2a)^{-i\epsilon}\cosh(\pi\epsilon) \tag{8.37}$$

Both K_m and K remove the ambiguity of dimension by nondimensionalizing r in $r^{i\epsilon}$ with $2a$ in the near-tip stress field. As a result, both have the same dimension as that of the classical stress intensity factor. All the previous definitions of stress intensity factor are acceptable as far as the near-tip state is concerned. With the definition of K by Sun and Jih [8-6], the stress intensity factors for the finite crack problem shown in Figure 8.2 become

$$
\begin{aligned}
K_1 &= \sqrt{\pi a}\left(\sigma_{yy}^{\infty} - 2\epsilon\sigma_{xy}^{\infty}\right)/\cosh(\pi\epsilon) \\
K_2 &= \sqrt{\pi a}\left(\sigma_{xy}^{\infty} + 2\epsilon\sigma_{yy}^{\infty}\right)/\cosh(\pi\epsilon)
\end{aligned}
\tag{8.38}
$$

Using the stress intensity factor definition in Eq. (8.36), the near-tip relative displacement field Eq. (8.29) along the crack surfaces becomes

$$
\begin{aligned}
&\left(u_y + iu_x\right)_{\theta=\pi} - \left(u_y + iu_x\right)_{\theta=-\pi} \\
&= \left(\frac{\kappa_1+1}{\mu_1} + \frac{\kappa_2+1}{\mu_2}\right)\frac{K_1 + iK_2}{4(1+2i\epsilon)}\sqrt{\frac{2r}{\pi}}\left(\frac{r}{2a}\right)^{i\epsilon}
\end{aligned}
\tag{8.39}
$$

Sun and Jih [8-6] have given the stress and displacement fields around an interface crack tip as follows:

$$
\begin{aligned}
(\sigma_{xx})_j &= \frac{K_1}{2\sqrt{2\pi r}}\left[\omega_j f_{xx}^{I} - \frac{1}{\omega_j}\cos\left(\theta - \overline{\Theta}\right)\right] \\
&\quad - \frac{K_2}{2\sqrt{2\pi r}}\left[\omega_j f_{xx}^{II} + \frac{1}{\omega_j}\sin\left(\theta - \overline{\Theta}\right)\right] \\
\left(\sigma_{yy}\right)_j &= \frac{K_1}{2\sqrt{2\pi r}}\left[\omega_j f_{yy}^{I} + \frac{1}{\omega_j}\cos\left(\theta - \overline{\Theta}\right)\right] \\
&\quad - \frac{K_2}{2\sqrt{2\pi r}}\left[\omega_j f_{yy}^{II} - \frac{1}{\omega_j}\sin\left(\theta - \overline{\Theta}\right)\right] \\
\left(\sigma_{xy}\right)_j &= \frac{K_1}{2\sqrt{2\pi r}}\left[\omega_j f_{xy}^{I} - \frac{1}{\omega_j}\sin\left(\theta - \overline{\Theta}\right)\right] \\
&\quad - \frac{K_2}{2\sqrt{2\pi r}}\left[\omega_j f_{xy}^{II} - \frac{1}{\omega_j}\cos\left(\theta - \overline{\Theta}\right)\right]
\end{aligned}
\tag{8.40}
$$

and

$$
\begin{aligned}
(u_x)_j &= \frac{K_1\sqrt{2\pi r}}{4\pi\mu_j}\left[\kappa_j\omega_j h_{11} - \frac{1}{\omega_j}h_{12} + \omega_j h_{13}\right] \\
&\quad + \frac{K_2\sqrt{2\pi r}}{4\pi\mu_j}\left[\kappa_j\omega_j h_{21} - \frac{1}{\omega_j}h_{22} + \omega_j h_{23}\right] \\
\left(u_y\right)_j &= \frac{K_1\sqrt{2\pi r}}{4\pi\mu_j}\left[\kappa_j\omega_j h_{21} - \frac{1}{\omega_j}h_{22} - \omega_j h_{23}\right] \\
&\quad + \frac{K_2\sqrt{2\pi r}}{4\pi\mu_j}\left[-\kappa_j\omega_j h_{11} + \frac{1}{\omega_j}h_{12} + \omega_j h_{13}\right]
\end{aligned}
\tag{8.41}
$$

where $j = 1, 2$ represent the quantities in material 1 and 2, respectively, and

$$\overline{\Theta} = \epsilon \ln\left(\frac{r}{2a}\right) + \frac{\theta}{2}$$
$$\omega_1 = \exp\left[-\epsilon\left(\pi - \theta\right)\right]$$
$$\omega_2 = \exp\left[\epsilon\left(\pi + \theta\right)\right]$$

$$f_{xx}^{I} = 3\cos\overline{\Theta} + 2\epsilon\sin\theta\cos\left(\theta + \overline{\Theta}\right) - \sin\theta\sin\left(\theta + \overline{\Theta}\right)$$
$$f_{xx}^{II} = 3\sin\overline{\Theta} + 2\epsilon\sin\theta\sin\left(\theta + \overline{\Theta}\right) + \sin\theta\cos\left(\theta + \overline{\Theta}\right)$$
$$f_{yy}^{I} = \cos\overline{\Theta} - 2\epsilon\sin\theta\cos\left(\theta + \overline{\Theta}\right) + \sin\theta\sin\left(\theta + \overline{\Theta}\right)$$
$$f_{yy}^{II} = \sin\overline{\Theta} - 2\epsilon\sin\theta\sin\left(\theta + \overline{\Theta}\right) - \sin\theta\cos\left(\theta + \overline{\Theta}\right)$$
$$f_{xy}^{I} = \sin\overline{\Theta} + 2\epsilon\sin\theta\sin\left(\theta + \overline{\Theta}\right) + \sin\theta\cos\left(\theta + \overline{\Theta}\right)$$
$$f_{xy}^{II} = -\cos\overline{\Theta} - 2\epsilon\sin\theta\cos\left(\theta + \overline{\Theta}\right) + \sin\theta\sin\left(\theta + \overline{\Theta}\right)$$

$$h_{11} = \frac{1}{1 + 4\epsilon^2}\left[\cos\left(\theta - \overline{\Theta}\right) - 2\epsilon\sin\left(\theta - \overline{\Theta}\right)\right]$$
$$h_{12} = \frac{1}{1 + 4\epsilon^2}\left[\cos\overline{\Theta} - 2\epsilon\sin\overline{\Theta}\right]$$
$$h_{13} = \sin\theta\sin\overline{\Theta}$$
$$h_{21} = \frac{1}{1 + 4\epsilon^2}\left[\sin\left(\theta - \overline{\Theta}\right) + 2\epsilon\cos\left(\theta - \overline{\Theta}\right)\right]$$
$$h_{22} = \frac{1}{1 + 4\epsilon^2}\left[-\sin\overline{\Theta} + 2\epsilon\cos\overline{\Theta}\right]$$
$$h_{23} = \sin\theta\cos\overline{\Theta}$$

8.3 CRACK SURFACE CONTACT ZONE AND STRESS OSCILLATION ZONE

In this section, the crack surface contact zone and the stress oscillation zone near an interface crack tip are analyzed using the oscillatory crack tip fields introduced in Sections 8.2 and 8.3. More precise analysis of crack surface contact considering crack surface friction under shear dominated loading will be provided in Section 8.7.

8.3.1 Crack Surface Contact Zone

The crack surface displacements Eq. (8.39) exhibit an oscillating character, that is, they change sign indefinitely when r approaches zero. This oscillatory nature means

that the upper and lower crack surfaces will overlap near the crack tip, which is physically unrealistic. The two crack surfaces are actually in contact near the tip. In order for the stress intensity factors based on the oscillatory crack tip fields Eq. (8.36) to predict interface fracture, the size of this contact zone must be much smaller than the crack length or any other in-plane dimensions of the cracked body (small-scale contact).

Although precise evaluation of the contact zone size requires consideration of the crack surface contact in the analysis of displacement field (see [8-7] through [8-8]), which will be discussed in Section 8.7, the crack tip oscillatory displacement solution Eq. (8.39) provides a reasonable estimate for the contact zone size if small-scale contact prevails. The near-tip relative displacement along the crack surfaces can be obtained from Eq. (8.39) as follows:

$$\begin{aligned}\Delta u_y &= u_y(r,\pi) - u_y(r,-\pi) \\ &= \frac{\sqrt{2r}}{4(1+4\epsilon^2)\sqrt{\pi}}\left(\frac{\kappa_1+1}{\mu_1}+\frac{\kappa_2+1}{\mu_2}\right)(K_1H_1 - K_2H_2) \\ \Delta u_x &= u_x(r,\pi) - u_x(r,-\pi) \\ &= \frac{\sqrt{2r}}{4(1+4\epsilon^2)\sqrt{\pi}}\left(\frac{\kappa_1+1}{\mu_1}+\frac{\kappa_2+1}{\mu_2}\right)(K_1H_2 + K_2H_1)\end{aligned} \tag{8.42}$$

where

$$\begin{aligned}H_1 &= \left[\cos\left(\epsilon\ln\left(\frac{r}{2a}\right)\right) + 2\epsilon\sin\left(\epsilon\ln\left(\frac{r}{2a}\right)\right)\right] \\ H_2 &= \left[\sin\left(\epsilon\ln\left(\frac{r}{2a}\right)\right) - 2\epsilon\cos\left(\epsilon\ln\left(\frac{r}{2a}\right)\right)\right]\end{aligned} \tag{8.43}$$

The contact zone size may be estimated by adopting r_c, the largest r at which the relative normal displacement given by Eq. (8.42) vanishes, that is,

$$K_1H_1 - K_2H_2 = 0$$

Substitution of Eq. (8.43) into this equation yields (Sun and Qian [8-9])

$$r_c = 2a\exp\left[\frac{1}{\epsilon}\left(\tan^{-1}\left(\frac{K_1+2\epsilon\cdot K_2}{K_2-2\epsilon\cdot K_1}\right)-\pi\right)\right] \tag{8.44}$$

Equation (8.44) represents the contact zone size for general crack problems. For an infinite bimaterial medium with a crack subjected to remote loading shown in Figure 8.2, Eq. (8.44) becomes

$$r_c = 2a\exp\left[-\frac{1}{\epsilon}\left(\frac{\pi}{2}+\psi\right)\right] \tag{8.45}$$

where ψ is the loading phase angle defined by

$$\sigma_{yy}^{\infty} + i\sigma_{xy}^{\infty} = Te^{i\psi}$$

Redefining the phase angle ψ as

$$\tan\psi = \frac{K_2}{K_1}$$

Eq. (8.44) can be rewritten in the following form:

$$\frac{r_c}{2a} = \exp\left[\frac{1}{\epsilon}\left(\tan^{-1}\left(\frac{1+2\epsilon\tan\psi}{\tan\psi - 2\epsilon}\right) - \pi\right)\right] \tag{8.46}$$

For the small-scale contact conditions to prevail, Rice [8-10] suggested that $r_c/(2a) \leq 0.01$. Using Eq. (8.46), this condition can be expressed as

$$\frac{1+2\epsilon\tan\psi}{\tan\psi - 2\epsilon} \leq \tan(\epsilon \ln 0.01)$$

8.3.2 Stress Oscillation Zone

The oscillatory nature of the crack tip stress field Eq. (8.36) implies that the normal stress σ_{yy} may become negative near the crack tip even if the cracked bimaterial is subjected to tension loading. To study the size of the stress oscillation zone, we consider the near-tip stress fields for a two-dimensional infinite medium with a center crack of size $2a$ subjected to remotely uniform tensile stress σ_{yy}^{∞} shown in Figure 8.2 (with $\sigma_{xy}^{\infty} = 0$).

The asymptotic crack tip stresses along the interface ahead of the crack tip for this problem can be obtained by substituting Eq. (8.38) into Eq. (8.36):

$$\sigma_{yy} = \frac{\sigma_{yy}^{\infty}}{\sqrt{2r/a}}\left[\cos\left(\epsilon\ln\frac{r}{2a}\right) - 2\epsilon\sin\left(\epsilon\ln\frac{r}{2a}\right)\right]$$

$$\sigma_{xy} = \frac{\sigma_{yy}^{\infty}}{\sqrt{2r/a}}\left[\sin\left(\epsilon\ln\frac{r}{2a}\right) + 2\epsilon\cos\left(\epsilon\ln\frac{r}{2a}\right)\right]$$

Let r_o and r_o^* denote the sizes of the oscillation zones of the normal stress and the shear stress, respectively. Without loss of generality, we assume $\epsilon > 0$. The size r_o for the normal stress σ_{yy} can be determined by finding the largest value of x at which $d\sigma_{yy}/dx = 0$ with the result

$$r_o = 2a\exp\left(-\frac{\pi}{2\epsilon}\right) \tag{8.47}$$

It is noted that r_o is the same as the crack surface contact zone size given in Eq. (8.45) (now $\psi = 0$). Similarly, by letting $d\sigma_{xy}/dx = 0$, we can find the oscillation zone size

r_o^* for the shear stress as

$$r_o^* = 2a \exp\left(-\frac{\pi}{\epsilon}\right) \tag{8.48}$$

These two equations indicate that the size of the oscillation zone for the shear stress is much smaller than that for the normal stress and the oscillation zone size depends on the parameter ϵ, which is uniquely expressed by Dundurs' parameter β in Eq. (8.23).

For the largest mismatch case of $\beta = 0.5$ ($\epsilon = 0.1748$), the size of the normal stress oscillation zone is evaluated as $r_o/a = 2.51 \times 10^{-4}$ and the shear stress oscillation zone size is $r_o^*/a = 3.15 \times 10^{-8}$. For $\beta = 0.2$, these lengths are evaluated as $r_o/a = 5.34 \times 10^{-11}$ and $r_o^* = 1.44 \times 10^{-21}$, respectively. Hence, except for extreme mismatch cases, the oscillation zone is very small as compared with the crack size.

Gautsen and Dundurs [8-11] obtained the stresses along the interface for the crack problem shown in Figure 8.2 (remote tensile load only) by considering the crack face contact in the near-tip region. The log-log plot of the normal and shear stresses ahead of the crack tip from the contact model [8-11] and the oscillatory model [8-3] are shown in Figures 8.4 and 8.5 for $\beta = 0.2$ and $\beta = 0.5$, respectively, where $\beta = 0.5$ stands for the largest mismatch of elastic constants.

It is clear from the figures that solutions from both models agree extremely well beyond $x/a = 10^{-4}$, except for the normal stress associated with $\beta = 0.5$. For this case, the normal stresses from the two models agree up to $x/a = r_o \approx 2.51 \times 10^{-4}$. This value turns out to be the size of the oscillation (or overlap) zone for the crack-tip normal stress. Because the stresses of the two models agree very well except in the small contact zone near the crack tip, the oscillatory crack tip fields may still be used as the basis for predicting interface fracture.

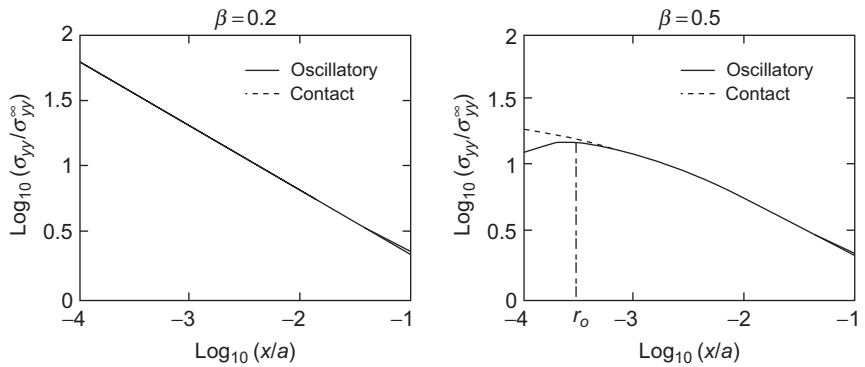

FIGURE 8.4

Normal stress distributions along the interface ahead of the crack with and without consideration of crack surface contact (adapted from Sun and Qian [8-9]).

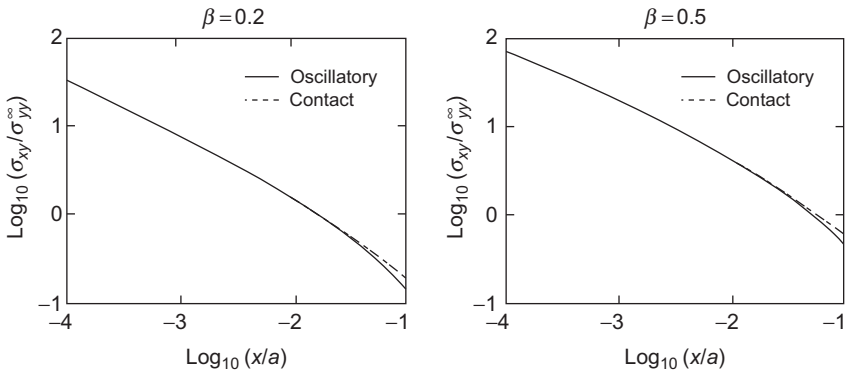

FIGURE 8.5

Shear stress distributions along the interface ahead of the crack with and without consideration of crack surface contact (adapted from Sun and Qian [8-9]).

8.4 ENERGY RELEASE RATE

Both Mode I and Mode II are, in general, present in interface cracks. Moreover, the energy release rates for the individual modes do not exist because of the oscillatory nature of the crack tip stress and displacement fields. Since the total energy release rate exists, the fracture criterion for interface cracks is usually given in terms of a critical value of the total energy release rate accompanied by a mode mixity $\tan^{-1}(K_{II}/K_I)$. Thus, in addition to the total energy release rate, both stress intensity factors must be calculated for fracture prediction.

8.4.1 Energy Release Rate

Due to the complication related to the oscillatory stress and displacement fields, the energy balance approach is more convenient for inteface fracture. Unlike the case for homogeneous materials, the Mode I and Mode II energy release rates do not exist for general bimaterial interface cracks (Sun and Jih [8-6]). Using the crack closure integral technique of Irwin [8-12], the Mode I and Mode II energy release rates may be defined as

$$G_1 = \lim_{\Delta a \to 0} \frac{1}{2\Delta a} \int_0^{\Delta a} \sigma_{yy}(x,0)\Delta u_y(\Delta a - x, \pi)dx$$
$$G_2 = \lim_{\Delta a \to 0} \frac{1}{2\Delta a} \int_0^{\Delta a} \sigma_{xy}(x,0)\Delta u_x(\Delta a - x, \pi)dx \tag{8.49}$$

where $\sigma_{xy}(x,0)$ and $\sigma_{yy}(x,0)$ are the stress fields when the crack tip is at $x=0$, and $\Delta u_x(\Delta a-x,\pi)$ and $\Delta u_y(\Delta a-x,\pi)$ are the relative displacements of the crack faces when the crack tip is at $x=\Delta a$.

The normal and shear stresses at the interface ahead of the crack tip ($x=0$) are obtained from Eq. (8.36) as

$$\begin{aligned}\sigma_{yy}(x,0)&=\frac{\cosh(\pi\epsilon)}{\sqrt{2\pi x}}\left[K_1(a)\cos\left(\epsilon\ln\frac{x}{2a}\right)-K_2(a)\sin\left(\epsilon\ln\frac{x}{2a}\right)\right]\\ \sigma_{xy}(x,0)&=\frac{\cosh(\pi\epsilon)}{\sqrt{2\pi x}}\left[K_1(a)\sin\left(\epsilon\ln\frac{x}{2a}\right)+K_2(a)\cos\left(\epsilon\ln\frac{x}{2a}\right)\right]\end{aligned}\tag{8.50}$$

Similarly, the relative displacements of crack faces behind the tip ($x=\Delta a$) can be obtained from Eq. (8.39) with the results

$$\begin{aligned}\Delta u_y(\Delta a-x,\pi)&=\frac{\sqrt{2(\Delta a-x)}}{4(1+4\epsilon^2)\sqrt{\pi}}\left(\frac{\kappa_1+1}{\mu_1}+\frac{\kappa_2+1}{\mu_2}\right)\\ &\quad\times[K_1(a+\Delta a)H_1-K_2(a+\Delta a)H_2]\\ \Delta u_x(\Delta a-x,\pi)&=\frac{\sqrt{2(\Delta a-x)}}{4(1+4\epsilon^2)\sqrt{\pi}}\left(\frac{\kappa_1+1}{\mu_1}+\frac{\kappa_2+1}{\mu_2}\right)\\ &\quad\times[K_1(a+\Delta a)H_2+K_2(a+\Delta a)H_1]\end{aligned}\tag{8.51}$$

where H_1 and H_2 are given in Eq. (8.43) with r replaced by $\Delta a-x$.

Substituting the preceding stresses and displacements into Eq. (8.49), we obtain the energy release rates as follows:

$$\begin{aligned}G_1&=\frac{1}{32}\left(\frac{\kappa_1+1}{\mu_1}+\frac{\kappa_2+1}{\mu_2}\right)\left(K_1^2+K_2^2\right)\\ &\quad+\lim_{\Delta a\to 0}\eta\left(1+\frac{\Delta a}{2a}+\cdots\right)\left[A_R\left(K_1^2-K_2^2\right)-2A_IK_1K_2\right]\\ G_2&=\frac{1}{32}\left(\frac{\kappa_1+1}{\mu_1}+\frac{\kappa_2+1}{\mu_2}\right)\left(K_1^2+K_2^2\right)\\ &\quad-\lim_{\Delta a\to 0}\eta\left(1+\frac{\Delta a}{2a}+\cdots\right)\left[A_R\left(K_1^2-K_2^2\right)-2A_IK_1K_2\right]\end{aligned}\tag{8.52}$$

where

$$\eta=\frac{\cosh(\pi\epsilon)}{8(1+4\epsilon^2)\pi}\left(\frac{\kappa_1+1}{\mu_1}+\frac{\kappa_2+1}{\mu_2}\right)\tag{8.53}$$

$$\begin{aligned}A_R&=\ \mathrm{Re}\{A\}\\ A_I&=-\mathrm{Im}\{A\}\end{aligned}$$

$$A = \frac{\sqrt{\pi}}{2}\left(\frac{1}{2}+i\epsilon\right)\left(\frac{\Delta a}{4a}\right)^{-2i\epsilon}\Gamma\left(\frac{1}{2}-i\epsilon\right)/\Gamma(1-i\epsilon) \tag{8.54}$$

in which $\Gamma(\ )$ is the Gamma function. It can be seen from these equations that the limits for A, and hence G_1 and G_2 as $\Delta a \to 0$ do not exist for general nonzero oscillation index ϵ. The total energy release rate G defined as $G_1 + G_2$, however, exists and is equal to

$$G = G_1 + G_2 = \frac{1}{16}\left(\frac{\kappa_1+1}{\mu_1}+\frac{\kappa_2+1}{\mu_2}\right)\left(K_1^2+K_2^2\right) \tag{8.55}$$

which agrees with the result obtained by Malyshev and Salganik [8-5].

8.4.2 Stress Intensity Factor Calculations

While the crack closure technique is convenient and efficient for calculating mixed mode energy release rates and stress intensity factors for homogeneous materials, no convergent energy release rates for Mode I and Mode II exist for interfacial cracks, which makes the conventional crack closure technique futile for stress intensity factor calculations.

To provide a scheme for calculation of stress intensity factors for interfacial cracks based on the energy release rate, Sun and Jih [8-6] and Sun and Qian [8-9] proposed to use modified energy release rates based on a finite crack extension Δa in the finite element calculation of stress intensity factors.

The modified energy release rates have the same expressions as in Eq. (8.49) but without taking the limit of $\Delta a \to 0$, that is,

$$\begin{aligned}\hat{G}_1 &= \frac{1}{2\Delta a}\int_0^{\Delta a}\sigma_{yy}(x,0)\Delta u_y(\Delta a - x,\pi)dx \\ \hat{G}_2 &= \frac{1}{2\Delta a}\int_0^{\Delta a}\sigma_{xy}(x,0)\Delta u_x(\Delta a - x,\pi)dx\end{aligned} \tag{8.56}$$

Substituting Eqs. (8.50) and (8.51) into the preceding equation and neglecting higher order terms in Δa yields

$$\begin{aligned}\hat{G}_1 &= \frac{1}{2}G + C\left[A_R\left(K_1^2-K_2^2\right)-2A_I K_1 K_2\right] \\ \hat{G}_2 &= \frac{1}{2}G - C\left[A_R\left(K_1^2-K_2^2\right)-2A_I K_1 K_2\right]\end{aligned} \tag{8.57}$$

where G is the total energy release rate given in Eq. (8.55), A_R and A_I are given in Eq. (8.54), and C is a constant given by

$$C = \frac{\cosh(\pi\epsilon)}{8(1+4\epsilon^2)\pi}\left(\frac{\kappa_1+1}{\mu_1}+\frac{\kappa_2+1}{\mu_2}\right)\left(1+\frac{\Delta a}{2a}\right) \tag{8.58}$$

By solving the two equations in Eq. (8.57) for K_1 and K_2, and neglecting the negative solution for K_1, Sun and Qian [8-9] obtained the stress intensity factors in terms of $\hat{G}_1$ and $\hat{G}_2$ as follows:

$$\begin{aligned} K_1 &= \sqrt{\frac{4A_RS+4A_I^2\frac{G}{D}\pm 4\sqrt{\left(A_RS+A_I^2\frac{G}{D}\right)^2-\left(A_R^2+A_I^2\right)S^2}}{8\left(A_R^2+A_I^2\right)}} \\ K_2 &= \frac{2A_RK_I^2-S}{2A_IK_I} \end{aligned} \tag{8.59}$$

where

$$\begin{aligned} S &= \frac{\hat{G}_1-\hat{G}_2}{2C}+\frac{A_RG}{D} \\ D &= \frac{1}{16}\left(\frac{\kappa_1+1}{\mu_1}+\frac{\kappa_2+1}{\mu_2}\right) \end{aligned}$$

Equation (8.59) indicates that, for one set of $\hat{G}_1$ and $\hat{G}_2$, two sets of solutions for K_1 and K_2 may exist. However, there is only one set of K_1 and K_2 that is physically meaningful. The correct K_1 and K_2 can be extracted using conditions on the crack surface displacements.

Use of Eqs. (8.57) and (8.59) to calculate stress intensity factors requires selection of crack extension length Δa. Δa can be selected to satisfy $\Delta a > r_o$, where r_o is the size of the oscillation zone given in Eq. (8.47), so that the normal crack opening is positive. At the same time, the sign of relative tangential crack surface displacement Δu_x can be determined easily from the finite element result. Hence, the displacement conditions for selecting the roots of K_1 and K_2 for interface cracks are

$$\Delta u_y(\Delta a) > 0, \quad sgn(\Delta u_x) \quad \text{determined by FEA}$$

Substitition of Eq. (8.42) into this equation yields the conditions for selecting K_1 and K_2:

$$\begin{aligned} K_1H_1 - K_2H_2 &> 0 \\ sgn(K_1H_2+K_2H_1) &= sgn(\Delta u_x) \quad \text{determined by FEA} \end{aligned}$$

Note that for the nonoscillation case ($\epsilon = 0$), there is only one pair of K_1 and K_2.

Besides the energy method introduced before, stress intensity factors for interfacial cracks can also be calculated using their relations with the near-tip displacements

in Eq. (8.42). Matos et al. [8-13] showed that the stress intensity factors obtained directly from these relations are not reliable. Depending on the location at which these crack surface displacements are taken, the stress intensity factors may vary appreciably. Recognizing that the individual crack surface displacements Δu_x and Δu_y obtained from finite element analysis may not be accurate, but the ratio $\Delta u_x/\Delta u_y$ seems to be more accurate, Sun and Qian [8-9] proposed to use this ratio to determine the stress intensity factor ratio K_2/K_1, which can be expressed in terms of displacement ratio $\Delta u_x/\Delta u_y$ as follows:

$$\frac{K_2}{K_1} = \frac{H_1 - H_2 \times \Delta u_y/\Delta u_x}{H_2 + H_1 \times \Delta u_y/\Delta u_x} \tag{8.60}$$

Stress intensity factors K_1 and K_2 can be obtained from this equation and the total energy release rate Eq. (8.55). Clearly, this displacement ratio scheme is more convenient to perform than the energy method.

Sun and Qian [8-9] calculated the stress intensity factors for a center crack of length $2a$ at the interface between two semi-infinite materials subjected to remote uniform tension σ_{yy}^{∞} and shear σ_{xy}^{∞} as shown in Figure 8.2. In the finite element calculations, the infinite plate was modeled by a panel of size 100×100 with a crack of length 2 ($a = 1$). The finite crack extension was taken as $\Delta a/a = 0.01$. The ratios of Poisson's ratios and Young's moduli of the two materials were $\nu_1/\nu_2 = 1$, and $E_1/E_2 = 10$ and 100. A state of plane stress was assumed.

Table 8.1 shows the finite element results using the energy method and the analytical solutions of Rice and Sih [8-3]. It is found that the average relative errors for K_1 and K_2 are less than 0.1% and 0.6%, respectively. The relatively higher error for K_2 is believed to be purely numerical resulting from a small $\hat{G}_2$ value.

Table 8.2 lists the finite element results using the displacement ratio method and the analytical solutions. Crack surface displacements at various locations were taken

Table 8.1 Stress Intensity Factors for a 100×100 Plane Stress Panel Subjected to Tensile and Shear Loading

		K_1			K_2		
E_1/E_2	$\sigma_{xy}^{\infty}/\sigma_{yy}^{\infty}$	Exact	Energy Method	Error (%)	Exact	Energy Method	Error (%)
10	0.0	1.6982	1.6976	0.04	−0.3185	−0.3195	0.30
	0.5	1.8575	1.8565	0.05	0.5306	0.5319	0.25
	1.0	2.0167	2.0175	0.04	1.3797	1.3711	0.19
100	0.0	1.6649	1.6642	0.04	−0.3790	−0.3793	0.08
	0.5	1.8544	1.8530	0.07	0.4535	0.4564	0.66
	1.0	2.0439	2.0456	0.09	1.2859	1.2815	0.34

Source: Adapted from Sun and Qian [8-9].

Table 8.2 Relative Errors of Stress Intensity Factors Using the Displacement Ratio Method for a 100×100 Plane Stress Panel with $E_1/E_2 = 100$ and $\sigma_{xy}^{\infty}/\sigma_{yy}^{\infty} = 1.0$

Element Number	First	Second	Third	Fourth	Fifth
x/a	0.01	0.02	0.03	0.04	0.05
Error for K_1 (%)	2.72	0.67	0.37	0.24	0.13
Error for K_2 (%)	6.46	1.54	0.82	0.48	0.19

Source: Adapted from Sun and Qian [8-9].

to compute the displacement ratios. It is again found that the relative errors for both K_1 and K_2 are less than 1.0% if the nodal displacements were taken at least two elements away from the crack tip.

8.5 FRACTURE CRITERION

In general, fracture of interfaces is inherently of mixed mode due to the material asymmetry. It is known from Chapter 5 that for mixed mode fracture in homogeneous materials, the crack growth path needs to be considered in a fracture criterion. For interface cracks, however, failure often occurs along the interface, that is, the crack growth direction is known. An interface crack may kink into one of the bulk materials if the interface toughness is relatively high, which will be discussed in Section 8.6. Due to the oscillatory nature of the interface crack tip fields, it is more convenient to use energy release rate to formulate fracture criteria for interface failure.

According to the energy release rate criterion, fracture occurs when the energy release rate reaches a critical value. The experiment by Cao and Evans [8-14] shows that the interface toughness for a given bimaterial system is not a constant, but depends on the mode mixity. The energy release rate criterion can thus be expressed as

$$G = G_c(\psi) \tag{8.61}$$

where G_c is the critical energy release rate and ψ is an appropriately defined phase angle. Hutchinson and Suo [8-15] provided some functional forms for the dependence of G_c on the phase angle. For the special case of $\epsilon = 0$ (nonoscillation), ψ may be uniquely defined by the stress intensity factors as follows:

$$\psi = \tan^{-1}\left(\frac{K_2}{K_1}\right) \tag{8.62}$$

For general bimaterial systems ($\epsilon \neq 0$), ψ may not be uniquely defined. This is because, from Eq. (8.31), the ratio of the near-tip shear stress σ_{xy} to the normal stress

σ_{yy} along the interface,

$$\left(\frac{\sigma_{xy}}{\sigma_{yy}}\right)_{\theta=0} = \frac{\mathrm{Im}\left[K_h r^{i\epsilon}\right]}{\mathrm{Re}\left[K_h r^{i\epsilon}\right]}$$

is a function of r, the distance from the crack tip, no matter how small r is. To define the mode mixity unambiguously, Rice [8-10] suggested a definition of stress intensity factor of the classical type denoted by $K_I + iK_{II}$,

$$K_I + iK_{II} = K_h \hat{r}^{i\epsilon} \tag{8.63}$$

where $\hat{r}$ is a reference length. The phase angle according to this stress intensity definition may be expressed as

$$\psi_r = \tan^{-1}\left[\frac{\mathrm{Im}(K_h \hat{r}^{i\epsilon})}{\mathrm{Re}(K_h \hat{r}^{i\epsilon})}\right] \tag{8.64}$$

which represents the mode mixity of the stress field at $r = \hat{r}$ if $\hat{r}$ falls within the K-dominance zone since

$$\psi_r = \tan^{-1}\left(\frac{\sigma_{xy}}{\sigma_{yy}}\right)_{r=\hat{r}}$$

As noted by Rice [8-10] and Hutchinson and Suo [8-15], the reference length $\hat{r}$ may be chosen arbitrarily within a range of length scales. It could be chosen based on the geometrical dimensions of the cracked body or a material length scale. If $\hat{r}$ is chosen as $2a$, the phase angle in Eq. (8.64) becomes

$$\psi_K = \tan^{-1}\left[\frac{\mathrm{Im}(K)}{\mathrm{Re}(K)}\right] = \tan^{-1}\left(\frac{K_2}{K_1}\right) \tag{8.65}$$

where $K = K_1 + iK_2$ is the stress intensity factor defined in Sun and Jih [8-6].

8.6 CRACK KINKING OUT OF THE INTERFACE

In the fracture criterion Eq. (8.61), the crack is assumed to extend along the interface between two dissimilar materials. The crack, however, may also kink into one of the two bulk materials depending on the loading conditions, material properties, and interface fracture toughness. Assume that an interface crack kinks into material 2 as shown in Figure 8.6.

When the kink length Δa is small compared with the original interface crack, the stress intensity factors K_I and K_{II} at the kink crack tip may be expressed in terms of the complex stress intensity factor at the main crack tip [8-16]:

$$K_I + iK_{II} = c(\omega, \alpha, \beta) K_h (\Delta a)^{i\epsilon} + \overline{d}(\omega, \alpha, \beta) \overline{K}_h (\Delta a)^{-i\epsilon} \tag{8.66}$$

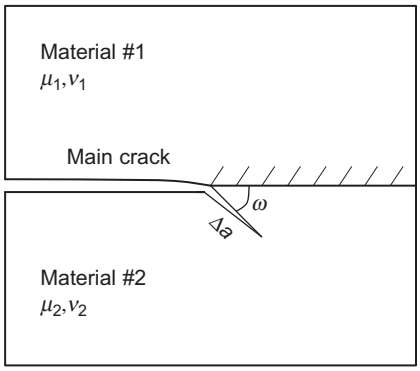

FIGURE 8.6

An interface crack kinking into material 2.

where ω is the kink angle, α and β are two Dundurs' parameters Eq. (8.22), and c and $\overline{d}$ are two dimensionless constants. The energy release rate at the kink crack tip is given by

$$G_{kink} = \frac{\kappa_2 + 1}{8\mu_2}\left(K_I^2 + K_{II}^2\right)$$

Using the relation Eq. (8.66), G_{kink} can be expressed in the following form:

$$\frac{G_{kink}}{G} = f(\omega, \alpha, \beta, \widetilde{\psi}) \tag{8.67}$$

where G is the energy release rate for crack extension along the interface, that is,

$$G = \frac{1}{16}\left(\frac{\kappa_1 + 1}{\mu_1} + \frac{\kappa_2 + 1}{\mu_2}\right) K_h \overline{K}_h$$

and $\widetilde{\psi}$ is a phase angle defined by

$$\widetilde{\psi} = \psi_r + \epsilon \ln\left(\frac{\Delta a}{\hat{r}}\right)$$

in which ψ_r is the phase angle defined in Eq. (8.64). He and Hutchinson [8-16] gave detailed numerical results of G_{kink}/G.

With the given loading parameter G_{kink}/G, the condition for the interface crack to kink into material 2 at an angle ω may be formulated as

$$\frac{G_{kink}(\omega, \alpha, \beta, \widetilde{\psi})}{G} > \frac{\Gamma_c}{G_c(\psi_r)}$$

where Γ_c is the critical energy release rate of material 2 and $G_c(\psi_r)$ is the interface toughness.

8.7 CONTACT AND FRICTION IN INTERFACIAL CRACKS

The oscillatory nature of stress and displacement fields near the tip of an interfacial crack implies contact of the crack surfaces, as discussed in Section 8.3. When the contact zone size is much smaller than the crack length and other in-plane dimensions such as in bimaterial cracks under Mode I loading, the oscillatory crack tip fields may still be used to predict interfacial fracture. However, the contact zone size may become comparable to the crack length if an interfacial crack is subjected to Mode II or shear-dominated loading. In this case, the crack tip fields are significantly altered especially if friction between the crack surfaces is present. This section introduces the fracture mechanics concepts for interfacial cracks considering crack face contact and friction.

8.7.1 Crack Tip Fields

For a crack in homogenous materials with friction or an interface crack without friction, there is always a square root singularity associated with the near-tip field. For an interfacial crack between two dissimilar isotropic materials with friction, however, the stress singularity is always weaker for a stationary crack under monotonic loading, that is, the stress exhibits a singularity of $r^{-\lambda}$ with $\lambda < 0.5$, as originally shown by Comninou [8-7].

The solution with consideration of crack face contact can be obtained basically following the asymptotic expansion procedure introduced by Williams [8-1]. as described in Section 8.1. The Airy stress functions in Comninou's solution are assumed to be in the following form:

$$\phi_j = r^{2-\lambda} F_j(\theta), \quad j = 1,2 \tag{8.68}$$

where (r,θ) are the polar coordinates centered at the crack tip as shown in Figure 8.1. The only difference between the previous form and that of Eq. (8.4) is in the definition of eigenvalue λ. From the stress functions the corresponding stress and displacement fields can be obtained for both materials. Note that with this definition of λ, the near-tip stress field is proportional to $r^{-\lambda}$. The difference in stress singularity between the frictional and frictionless interface cracks is due to the differences in boundary conditions along the crack surfaces.

The boundary conditions along the interface are given as follows. Ahead of the crack tip ($\theta = 0$), the displacements and stresses must be continuous, that is,

$$\begin{aligned} (u_r)_1 &= (u_r)_2, \quad \theta = 0 \\ (u_\theta)_1 &= (u_\theta)_2, \quad \theta = 0 \\ (\sigma_{r\theta})_1 &= (\sigma_{r\theta})_2, \quad \theta = 0 \\ (\sigma_{\theta\theta})_1 &= (\sigma_{\theta\theta})_2, \quad \theta = 0 \end{aligned} \tag{8.69}$$

Behind the crack tip ($\theta = \pm\pi$), the displacements and tractions of the upper and lower crack surfaces must satisfy the following continuity and equilibrium equations:

$$\begin{aligned}
&(u_\theta)_1|_{\theta=\pi} = (u_\theta)_2|_{\theta=-\pi} \\
&(\sigma_{\theta\theta})_1|_{\theta=\pi} = (\sigma_{\theta\theta})_2|_{\theta=-\pi} \\
&(\sigma_{r\theta})_1|_{\theta=\pi} = (\sigma_{r\theta})_2|_{\theta=-\pi} = -\mu(\sigma_{\theta\theta})_1|_{\theta=\pi} \\
&(\sigma_{\theta\theta})_1|_{\theta=\pi} \leq 0, \qquad (\sigma_{\theta\theta})_2|_{\theta=-\pi} \leq 0
\end{aligned} \tag{8.70}$$

where μ denotes the coefficient of friction. Note that the signs of the shear stresses depend on the direction of slip. To distinguish the directions of slip, the value of μ can also assume negative values.

For instance, a positive μ gives positive shear stresses on both upper and lower surfaces thus indicating the upper medium moves relative to the lower medium in the positive x-direction. A negative μ indicates a slip of the crack surfaces in the opposite direction. These conditions can be expressed in terms of the stress and displacement components with respect to the Cartesian coordinate system as follows:

$$\begin{aligned}
&\sigma_{yy}(r, \pm\pi) < 0 \\
&\sigma_{xy}(r, \pm\pi) = -\mu\sigma_{yy}(r, \pm\pi) \\
&sgn(\mu) = sgn(\Delta u_x)
\end{aligned} \tag{8.71}$$

where $\Delta u_x(r) = u_x(r, \pi) - u_x(r, -\pi)$ is the relative displacement in the x-direction between the upper and lower crack surfaces.

The two sets of boundary conditions given by Eqs. (8.69) and (8.70) yield eight homogeneous equations for the eight unknown constants in the solutions for $F_j(\theta)$. For a nontrivial solution to exist, the determinant of the coefficient matrix of the system of eight equations must vanish, that is,

$$\sin^3(\lambda\pi)\,[\cos(\lambda\pi) - \mu\beta\sin(\lambda\pi)] = 0 \tag{8.72}$$

where β is a Dundurs' parameter given by Eq. (8.22). Clearly, $\lambda = 0$ is a root of the characteristic Eq. (8.72) and can be ignored as it yields a uniform state of stress. The solution for λ that leads to singular stresses must be obtained from setting the second term in Eq. (8.72) equal to zero with the result

$$\cot(\lambda\pi) = \mu\beta \tag{8.73}$$

The near-tip stress field along the bimaterial interface and the relative crack surface sliding displacement in plane strain can be calculated from the stress function. In terms of the stress and displacement components with respect to the Cartesian

coordinate system we have

$$\begin{aligned}\sigma_{xy}(r,0) &= K_{II}(2\pi r)^{-\lambda}\\ \sigma_{xy}(r,\pm\pi) &= K_{II}(2\pi r)^{-\lambda}\cos(\lambda\pi)\\ \sigma_{yy}(r,0) &= 0\\ \sigma_{yy}(r,\pm\pi) &= -K_{II}\beta(2\pi r)^{-\lambda}\sin(\lambda\pi)\end{aligned} \tag{8.74}$$

and

$$\Delta u_x(r) = u_x(r,\pi) - u_x(r,-\pi) = \frac{\gamma K_{II}\sin(\lambda\pi)}{2(1-\lambda)(2\pi)^{\lambda}} r^{1-\lambda} \tag{8.75}$$

in which the generalized stress intensity factor is defined as

$$K_{II} = \lim_{r\to 0}(2\pi r)^{\lambda}\sigma_{xy}(r,0) \tag{8.76}$$

and

$$\gamma = \frac{(3-4\nu_1)(1-\beta)+(1+\beta)}{2\mu_1} + \frac{(3-4\nu_2)(1+\beta)+(1-\beta)}{2\mu_2}$$

The singularity index λ in the stresses Eq. (8.74) is obtained from Eq. (8.73). It is easy to see that λ is 0.5 if β or μ is zero, which corresponds to homogenous materials or the frictionless condition, respectively. If $\mu\beta > 0$, then $\lambda < 0.5$ and the stress singularity is weaker than the inverse square root singularity. On the other hand, $\lambda > 0.5$ if $\mu\beta < 0$, and then a stronger singularity exists.

It was noted by Comninou and Dundurs [8-8] that the problem of an interface crack with friction is a linear process in the context of monotonic loading. In this context, the energy released for a crack extension Δa can be obtained using Irwin's crack closure integral. Because of the contact of crack surfaces, only Mode II fracture mode is present. Sun and Qian [8-17] obtained the total energy release rate associated with a virtual crack extension Δa as follows:

$$\begin{aligned}\hat{G}(\Delta a) &= \frac{1}{2\Delta a}\int_0^{\Delta a}\left[\sigma_{xy}(r,0) - \sigma_{xy}(\Delta a - r,0)\right]\Delta u_x(\Delta a - r)dr\\ &= \frac{\gamma K_{II}^2\sin(\lambda\pi)}{4(1-\lambda)(2\pi)^{2\lambda}}(\Delta a)^{1-2\lambda}\left[\frac{\Gamma(2-\lambda)\Gamma(1-\lambda)}{\Gamma(3-2\lambda)} - \frac{\cos(\lambda\pi)}{2(1-\lambda)}\right]\end{aligned} \tag{8.77}$$

in which Γ is the gamma function. The conventional strain energy release rate is defined as

$$G = \lim_{\Delta a\to 0}\hat{G}(\Delta a)$$

In the crack closure integral of Eq. (8.77), the term $\sigma_{xy}(r,0)$ is the interfacial shear stress ahead of the crack tip, and $\sigma_{xy}(\Delta a - r,0)$ is the frictional shear stress behind the crack tip. During the crack extension of Δa, the shear stress initially ahead of the crack tip reduces to that of the frictional shear stress behind the crack tip after the assumed crack extension. Thus, the energy release rate of Eq. (8.77) can be interpreted as the total energy release rate less the frictional energy dissipation rate.

It is seen from Eq. (8.77) that the energy release rate $\hat{G}(\Delta a)$ vanishes as $\Delta a \to 0$ if $\lambda < 0.5$. Consequently, G cannot be used as a parameter in the fracture criterion. On the other hand, for $\Delta a = \Delta a_0 \neq 0$, $\hat{G}(\Delta a_0)$ is uniquely related to the stress intensity factor K_{II} and, thus, to the near-tip stress field. By selecting a proper characteristic crack closure distance Δa_0, it seems possible to use $\hat{G}(\Delta a_0)$ as a fracture parameter when friction is present.

8.7.2 Finite Element Procedure for Energy Calculation

Analytical solutions for interfacial cracks with frictional sliding are extremely difficult to obtain. Numerical methods such as the finite element method are necessary for practical applications. Sun and Qian [8-17] developed a finite element procedure to calculate the energy release rate $\hat{G}(\Delta a)$ and the energy dissipation due to friction during crack extension. This procedure is based on crack tip nodal forces and displacements. To separate the energy release from the frictional energy dissipation at the crack tip, the elastic nodal force must be separated from the frictional nodal force that results from the frictional traction on the crack surfaces.

For illustration purposes, assume that the crack tip is modeled using four-noded plane strain (or plane stress) elements as shown in Figure 8.7. To facilitate friction as well as nodal release, interface elements INTER2 in the commercial code ABAQUS are used along the interface ahead and behind the crack tip. Let $F_x^{(1)}$ and $F_y^{(1)}$ be the horizontal and vertical nodal forces, respectively, at the crack tip node in the loaded medium just before crack extension. The crack extension is simulated by releasing the crack tip node into two separate nodes a and b, allowing frictional sliding. The relative sliding of the nodes a and b (see Figure 8.7) is denoted by Δu_x.

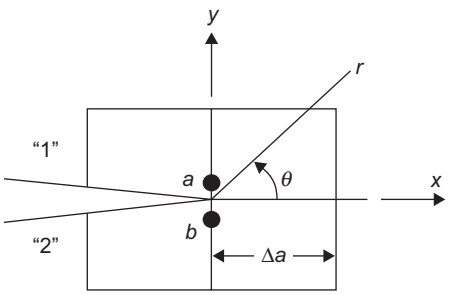

FIGURE 8.7

A crack along a bimaterial interface and the finite elements around the crack tip.

The elastic restoring nodal force at node a before crack extension is $F_x^{(1)} - \mu F_y^{(1)}$. Using Irwin's crack closure concept, the energy release rate for a crack extension of Δa is

$$\hat{G}(\Delta a) = \frac{1}{2\Delta a}\left(F_x^{(1)} - \mu F_y^{(1)}\right)\Delta u_x \tag{8.78}$$

During the assumed crack extension, the total dissipation energy rate associated with crack surface friction is given by

$$G_d(\Delta a) = G_d^N(\Delta a) + G_d^e(\Delta a) \tag{8.79}$$

where $G_d^N(\Delta a)$ is the portion of the dissipation energy rate produced by the newly formed crack surfaces, and $G_d^e(\Delta a)$ is the portion produced by the existing crack surfaces that are in contact. $G_d^N(\Delta a)$ can be determined from the following equation:

$$G_d^N(\Delta a) = \frac{1}{2\Delta a}\left(\mu F_x^{(1)} + \mu F_y^{(2)}\right)\Delta u_x$$

where $F_y^{(2)}$ is the vertical crack tip nodal force after crack extension. The calculation of $G_d^e(\Delta a)$ is similar to that of $G_d^N(\Delta a)$ and should include all the nodes in the contact region before crack extension.

A numerical example presented in Sun and Qian [8-17] is reproduced here. A center crack lying between two dissimilar isotropic media under remote shear loading τ (see Figure 8.8) was used to examine the accuracy of the finite element technique.

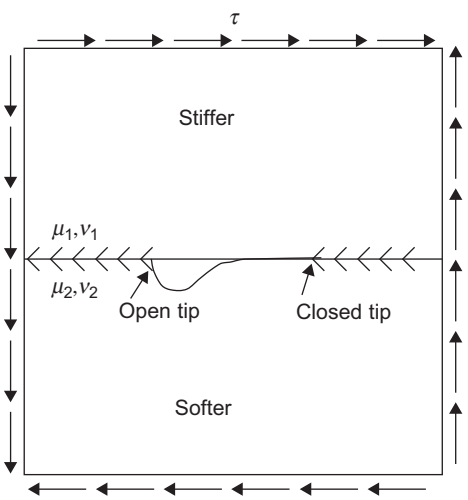

FIGURE 8.8

A cracked bimaterial panel, 20 m × 20 m, under remote shear loading.

Table 8.3 Comparison of Stress Intensity Factor K_{II} from Sun and Qian [8-17] and K_{II}^d Obtained by Comninou and Dunders [8-8] $\left(\overline{K}_{II} = \left(1+\mu^2\beta^2\right)K_{II}/\tau(2a)^{\lambda},\ \mu = 0.5,\ \beta = 0.5\right)$

$\Delta a/a$	$\overline{K}_{II}$ [8-17]	Error $\left\lvert\left(K_{II} - K_{II}^d\right)/K_{II}^d\right\rvert$
3.18×10^{-2}	0.9723	1.28%
1.59×10^{-2}	0.9720	1.25%
7.96×10^{-3}	0.9724	1.29%
3.98×10^{-3}	0.9737	1.42%

The commercial code ABAQUS was used to perform the analysis. The size of the medium was 20 m × 20 m with a crack of 2 m. A similar problem of an infinite bimaterial medium was also investigated by Comninou and Dundurs [8-8] using the elastic dislocation approach. The stress intensity factor obtained by calculating the energy release rate $\hat{G}(\Delta a)$ and using the relation Eq. (8.77) for the closed crack tip (right tip in Figure 8.8) is given together with those from Comninou and Dundurs [8-8] in Table 8.3. The agreement between these two methods is excellent. The slight difference is believed to be due to the finite size effect of the medium considered in Sun and Qian [8-17] in contrast to the infinite medium assumed by Comninou and Dundurs [8-8].

8.7.3 Fracture Criterion

The finite element procedure presented in the previous section is used to study the interfacial crack under shear loading as shown in Figure 8.8. The dimensions of the bimaterial medium are 20 m × 20 m with a half crack length $a = 1$ m. The applied shear stress τ is assumed to be 0.12 MPa. The material constants are $\mu_1 = 35$ MPa, $\mu_2 = 0.35$ MPa, and $\nu_1 = \nu_2 = 0$. These material constants yield a Dundurs' parameter of $\beta = 0.49$.

The relative crack surface normal displacements for $\mu = 0.2$ and 0.5, respectively, are shown in Figure 8.9. It is seen that there is a sizable contact zone near the right tip $(x/a = 1)$ while the crack is open at the left tip $(x/a = -1)$. The length of contact does not seem to be affected much by the coefficient of friction. For $\mu = 0.0$, 0.5, and 1.0 together with $\beta = 0.5$, the contact zone sizes normalized with half crack size are 0.655, 0.76, and 0.83, respectively [8-8]. Theoretically, there is an extremely small contact zone at the open left tip. However, this contact zone is so small that the left crack tip can be treated as an open crack with the classical oscillatory stress field [8-9].

The finite extension strain energy release rate $\hat{G}(\Delta a)$, dissipation energy rate $G_d(\Delta a)$, and total energy release rate $\hat{G}(\Delta a) + G_d(\Delta a)$ for the problem of Figure 8.8 with $\mu = 0.5$ corresponding to various crack extensions are shown in Figures 8.10 and 8.11 for the open (left) and closed (right) crack tips, respectively. At the left crack tip,

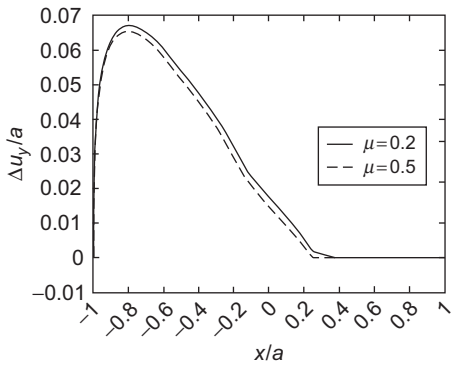

FIGURE 8.9

Relative crack surface normal displacement; a is half crack length (adapted from Sun and Qian [8-17]).

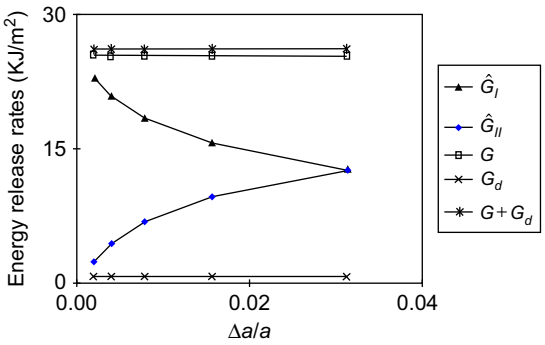

FIGURE 8.10

Finite extension energy release rates at the open crack tip (adapted from Sun and Qian [8-17]).

the contact zone r_c/a is usually around 10^{-5} to 10^{-7} and can be virtually treated as an open crack tip. The modified crack closure technique can therefore be applied to calculate the energy release rates.

It is seen in Figure 8.10 that individual finite extension strain energy release rates $\hat{G}_I$ and $\hat{G}_{II}$ are Δa-dependent, while the total strain energy release rate $G = \hat{G}_I + \hat{G}_{II}$ as well as the dissipation energy rate G_d remain constant for different crack extensions. It is noted that the dissipation energy rate is fairly small compared with energy release rate. This indicates that the frictional effect on the open crack tip is fairly small. It can also be shown that the stress distribution ahead of the open crack tip is very close to those of the oscillatory solution obtained based on the traction-free

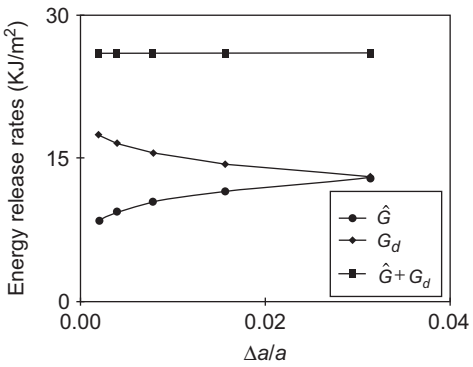

FIGURE 8.11

Finite extension energy release rates at the closed crack tip in the panel shown in Figure 8.8 for $\mu = 0.5$ (adapted from Sun and Qian [8-17]).

crack surface condition. It is concluded that frictional effect at the open crack tip is negligible. All existing approaches for the calculation of fracture parameters for bimaterial interfacial cracks are thus applicable (e.g., see [8-9]).

As for the fracture behavior at the closed crack tip (the right tip), it is clearly seen in Figure 8.11 that the finite extension strain energy release rate $\hat{G}$ (which is Mode II) decreases, and the dissipation energy rate G_d increases, while the total energy release rate $\hat{G} + G_d$ remains constant when crack extension decreases. The numerical results [8-17] indicate that the work done by the external force during the crack extension of Δa is equal to the sum of the increase of the strain energy in the cracked body, the strain energy released $\hat{G}\Delta a$, and the energy dissipated on the crack surfaces $G_d \Delta a$. As $\Delta a \to 0$, the work done is then equal to the gain in the strain energy of the cracked body plus the energy dissipated by friction.

Recall the relationship between energy release rate $\hat{G}$ and crack extension Δa in Eq. (8.77); energy release rate indeed decreases and eventually vanishes when Δa approaches zero due to the weak stress singularity. The energy release rate is therefore Δa-dependent, while the increase of dissipation energy rate makes up the decrease of energy release rate for total energy balance when Δa decreases. The implication of decreasing energy release rate (as $\Delta a \to 0$) is that the classical energy release rate concept is no longer valid because of its vanishing value. Consequently, an energy release rate associated with a finite crack extension is needed to quantify the weak singular stress field ahead of the crack tip.

The decreasing behavior of energy release rate was also noticed by Stringfellow and Freund [8-18] who computed the J-integral for the frictional sliding fracture in a thin film on a substrate. It was pointed out later by Deng [8-19] that the path independence of the J-integral no longer exists due to the crack surface traction resulting from friction, and the J-integral for a vanishingly small contour becomes zero indicating strain energy release rate also vanishes.

In view of the foregoing, Sun and Qian [8-17] proposed a fracture criterion using the energy release rate of a characteristic crack extension as a fracture toughness parameter, that is,

$$\hat{G}(\Delta a_0) = \frac{\Delta W_e}{\Delta a} - G_d(\Delta a_0) - \frac{\Delta U}{\Delta a} = \hat{G}_c \tag{8.80}$$

where ΔW_e, ΔU, and $G_d(\Delta a_0)$ are the external work done, strain energy change, and the dissipation energy rate for a crack extension of Δa_0, respectively. It is seen from Eq. (8.77) that for a fixed Δa_0 the finite extension energy release rate $\hat{G}$ has a unique relation with the generalized stress intensity factor K_{II}. The fracture criterion given by Eq. (8.80) states that the interfacial crack would grow if the near-tip stress field reaches a certain critical state.

8.7.4 Effect of Compressive Loading

An open crack may be forced to close if compressive loads normal to the crack surfaces are applied in addition to the shear load. An example is the residual stresses between the fiber and matrix in a composite resulting from the mismatch of coefficients of thermal expansion. Theoretically, the open region of the crack cannot be completely closed by externally applied compression. However, if the open crack is almost closed due to compressive loads, then the associated near-tip stress field is dominated by a singularity stronger than $\lambda = 0.5$, as discussed by Qian and Sun [8-20].

For this type of "closed" interfacial crack, the strain energy release rate for a finite extension Δa is also given by Eq. (8.77). It is obvious that if $\lambda > 0.5$, then $\hat{G}$ becomes unbounded as $\Delta a \to 0$. Consequently, the intrinsic interfacial fracture toughness must be measured in terms of the finite extension strain energy release rate $\hat{G}$ for a characteristic distance a_0. However, the toughnesses of the two closed interfacial cracks with stronger and weaker singularities, respectively, should not be interchanged, because they correspond to different critical near-tip stress states.

References

[8-1] M.L. Williams, The stresses around a fault or crack in dissimilar media, Bull. Seismol. Soc. Am. 49 (1959) 199–204.

[8-2] J. Dundurs, Edge-bonded dissimilar orthogonal elastic wedges under normal and shear loading, J. Appl. Mech. 36 (1969) 650–652.

[8-3] J.R. Rice, G.C. Sih, Plane problems of cracks in dissimilar media, J. Appl. Mech. 32 (1965) 418–423.

[8-4] J.W. Hutchinson, M. Mear, J.R. Rice, Crack paralleling an interface between dissimilar materials, J. Appl. Mech. 54 (1987) 828–832.

[8-5] B.M. Malysev, R.L. Salganik, The strength of adhesive joints using the theory of cracks, Int. J. Fract. 1 (1965) 114–127.

[8-6] C.T. Sun, C.J. Jih, On strain energy release rate for interfacial cracks in bimaterial media, Eng. Fract. Mech. 28 (1987) 13–20.

[8-7] M. Comninou, Interface crack with friction in the contact zone, J. Appl. Mech. 44 (1977) 780–781.

[8-8] M. Comninou, J. Dundurs, Effect of friction on the interface crack loaded in shear, J. Elast. 10 (1980) 203–212.

[8-9] C.T. Sun, W. Qian, The use of finite extension strain energy release rates in fracture of interfacial cracks, Int. J. Sol. Struct. 34 (1997) 2595–2609.

[8-10] J.R. Rice, Elastic fracture mechanics concepts for interficial cracks, J. Appl. Mech. 55 (1988) 98–103.

[8-11] A.K. Gautsen, J. Dundurs, The interface crack in a tension field, J. Appl. Mech. 54 (1987) 93–98.

[8-12] G.R. Irwin, Analysis of stresses and strains near the end of a crack traversing a plate, J. Appl. Mech. 24 (1957) 361–364.

[8-13] P.P.L. Matos, R.M. McMeeking, P.G. Charalamibides, D. Drory, A method for calculating stress intensities in bimaterial fracture, Int. J. Fract. 40 (1989) 235–254.

[8-14] H.C. Cao, A.G. Evans, An experimental study of the fracture—resistance of bimaterial interfaces, Mech. Mater. 7 (1989) 295–304.

[8-15] J.W. Hutchinson, and Z. Suo, Mixed mode cracking in layered materials, Adv. Appl. Mech. 29 (1992) 63–187.

[8-16] M.-Y. He, J.W. Hutchinson, Kinking of a crack out of an interface, J. Appl. Mech. 56 (1989) 270–278.

[8-17] C.T. Sun, W. Qian, A treatment of interfacial cracks in the presence of friction, Int. J. Fract. 94 (1998) 371–382.

[8-18] R.G. Stringfellow, L.B. Freund, The effect of interfacial friction on the buckle-driven spontaneous delamination of a compressed thin film, Int. J. Sol. Struct. 30 (1993) 1379–1395.

[8-19] X. Deng, Mechanics of debonding and delamination in composites: Asymptotic studies, Compos. Eng. 5 (1995) 1299–1315.

[8-20] W. Qian, C.T. Sun, Frictional interfacial crack under combined shear and compressive loading, Compos. Scie. Technol. 58 (1998) 1753–1761.

PROBLEMS

8.1 Calculate the two Dundurs' parameters for the following two pairs of materials: (1) Glass/epoxy with $E_1 = 70$ GPa, $\nu_1 = 0.2$ (glass) and $E_2 = 2$ GPa, $\nu_2 = 0.4$ (epoxy); (2) Al_2O_3/aluminum with $E_1 = 350$ GPa, $\nu_1 = 0.25$ (Al_2O_3) and $E_2 = 70$ GPa, $\nu_2 = 0.33$ (aluminum).

8.2 Derive the stress intensity factors for a semi-infinite interface crack subjected to uniform pressure p along part of the crack faces as shown in Figure 8.12.

8.3 Derive the relationship between the energy release rate and the stress intensity factor for Mode III interface cracks.

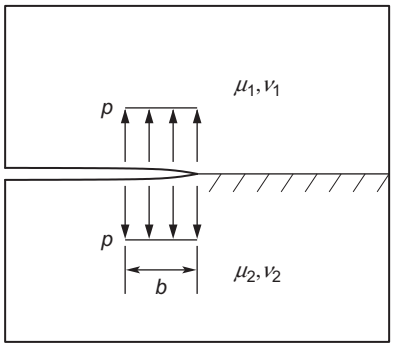

FIGURE 8.12

A semi-infinite interface crack subjected to pressure p along part of the crack faces.

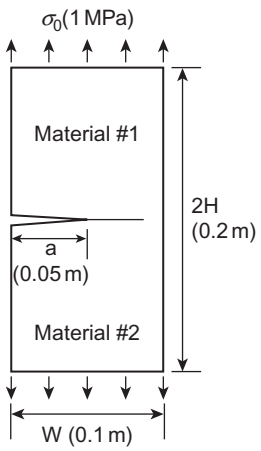

FIGURE 8.13

An edge interface crack in a bimaterial plate subjected to uniform tension.

8.4 Use plane strain or plane stress two-dimensional finite element to model the plate with an interfacial crack loaded as shown in Figure 8.13 The material properties of Material #1 and Material #2 are $E_1 = 210$ GPa, $\nu_1 = 0.3$ and $E_2 = 210$ GPa, $\nu_2 = 0.1$, respectively. Calculate G_I and G_{II} using the modified crack closure method. Check the convergence and the crack surface displacement near the crack tip.